Supporting Information

An Effective Design Strategy for Aggregation-Induced Emission and Thermally Activated Delayed Fluorescence Emitters Achieving 18% External Quantum Efficiency Pure Blue OLEDs with Extremely Low Roll-Off

Jinshan Wang,[†] *Jianfeng Zhang,*[*,‡] *Cuifeng Jiang,*[†] *Chuang Yao,*[*,§] *Xinguo Xi*[*,†]

[†] School of Materials Science and Engineering, Yancheng Institute of Technology, Yancheng 224051, P. R. China

[‡]School of Physics and Optoelectronic Engineering, Guangdong University of Technology, Guangzhou 510006, P. R. China

[§]Chongqing Key Laboratory of Extraordinary Bond Engineering and Advance Materials Technology (EBEAM), Yangtze Normal University, Chongqing 408100, P. R. China

Corresponding Author:

E-mail: zhangjianfeng@gdut.edu.cn (Jianfeng Zhang), yaochuang@yznu.cn (Chuang Yao) xxg@ycit.cn (Xinguo Xi)

Contents

1. General Information

All reactants and solvents used for the synthesis were commercially available and used without further purification unless otherwise specified. ^{1}HNMR and ^{13}CNMR spectra were recorded on a Bruker AVANCE III HD 400 MHz spectrometer operating at 300 and 100 MHz, respectively, using tetramethylsilane (TMS) as the internal standard. Matrix assisted laser desorption ionization/Time-of-flight (MALDI/TOF) mass spectra were performed on a AUTO FLEX III analyzer. Cyclic voltammetry (CV) was measured on a CHI-604E electro-chemical workstation with three-electrode system at a scan rate of 100 mV s^{-1}, in which glassy carbon electrode, Pt wire electrode and Ag/AgCl electrode as working electrode, counter electrode and reference electrode, respectively. A solution of tetra-*n*-butylammonium hexafluorophosphate (Bu_4NPF_6) (0.1 M) in dichloromethane (DCM) was used as electrolyte and the concentration of emitters was 1.0 × 10^{-3} M. The reference electrode was calibrated using the ferrocene/ferrocenium (Fc/Fc^{+}) redox couple as an external standard. Highest occupied molecular orbital (HOMO) energy level was determined from the onset potential of oxidation by cyclic voltammetry, $E_{HOMO}=-(E_{onset}+4.4)$ eV; while lowest unoccupied molecular orbital (LUMO) energy level can be calculated using E_{HOMO} and optical band gap (E_g), $E_{LUMO}=E_{HOMO}+E_g$. Thermogravimetric analysis (TGA) and differential scanning calorimetry (DSC) measurements were conducted under nitrogen atmosphere at a heating of rate 10 °C/min performed using a NETZSCH STA449F5 Jupiter Synchronous thermal analyzer. Ultraviolet-visible (UV-vis) absorption and photoluminescence (PL) emission spectra were recorded with a Hitachi U-3900H spectrophotometer and Hitachi F-7000

fluorescence spectrometer, respectively. The PL lifetimes and absolute photoluminescent quantum yield of emitters in film were measured in an integrating sphere on an Edinburgh FLS920 fluoro-spectrophotometer. Single crystals were grown in the mixtures of dichloromethane/methanol, and single crystal X-ray diffraction intensity data were collected at 293 K on Bruker Smart APEX II X-ray diffractometer equipped with a graphite-monochromated Cu-Kα radiation source (λ = 1.54184 Å). The structures were solved by a direct method and refined by full-matrix least squares on F^2 using the SHELX program.

2. Theoretical Calculation

The groundstate geometries and electronic properties of ICZ-DPS and ICZ-BP were optimized and calculated using the density function theory (DFT) method with B3LYP/6-31 G* basis set level by Gaussian 09. The molecular orbitals were visualized with GaussView 5.0. The singlet and triplet states were calculated using time-dependent density functional theory (TD-DFT) method at the B3LYP/6-31 G* level.

3. Devices Fabrication and Characterization

ITO-coated glass (10 Ω sq^{-1}) substrates were pre-cleaned carefully before UV-ozone treatment for 6 min. The devices were fabricated by vacuum depositing the materials at a pressure of 5 × 10^{-4} Pa. The organic layers were thermally evaporated at a rate of 1~2 Å s^{-1}, while 0.1 Å s^{-1} for LiF, and 3~5 Å s^{-1} for Al, respectively. The emission area of the devices is 2 mm×2 mm as shaped by the overlapping area of the anode and cathode. Both materials are further purified by temperature-gradient vacuum sublimation after column chromatography before OLEDs device fabrication by vacuum deposition. The current density-voltage characteristics, and luminance of the devices were measured with a Keithley 2400 source meter and a calibrated silicon photodiode. The electroluminescence spectra and luminance of the devices were obtained on a PR650 spectrometer. Efficiencies of devices were calculated using EL spectra and current, assuming the devices were Lambertian light sources. All the

device fabrication and characterization were performed at room temperature under ambient laboratory conditions.

4. Estimation of the Basic Photophysical Data

The rate constants and quantum efficiencies were determined using the following equations according to Adachi's method. [1−5]

$$\Phi_p = \Phi_{PL} R_p \quad (1)$$

$$\Phi_d = \Phi_{PL} R_d \quad (2)$$

$$k_F = \Phi_p / \tau_p \quad (3)$$

$$k_p = 1/\tau_p = k_F + k_{nr}^S + k_{ISC} \quad (4)$$

$$k_d = 1/\tau_d = k_{nr}^T + [1 - k_{ISC}/(k_F + k_{ISC})]k_{RISC} \quad (5)$$

$$k_{RISC} = (k_p k_d \Phi_d)/(k_{ISC} \Phi_p) \quad (6)$$

$$\Phi_{PL} = k_F/(k_F + k_{nr}^S) \quad (7)$$

$$\Phi_P = k_F/(k_F + k_{nr}^S + k_{ISC}) = k_F/k_p \quad (8)$$

$$\Phi_{ISC} = k_{ISC}/(k_F + k_{nr}^S + k_{ISC}) = k_{ISC}/k_p = 1 - \Phi_p - \Phi_{nr}^S \quad (9)$$

$$\Phi_{RISC} = \Phi_d/\Phi_{ISC} \quad (10)$$

$$\Phi_{nr}^S = k_{nr}^S/(k_F + k_{nr}^S + k_{ISC}) \quad (11)$$

5. Figures and Tables

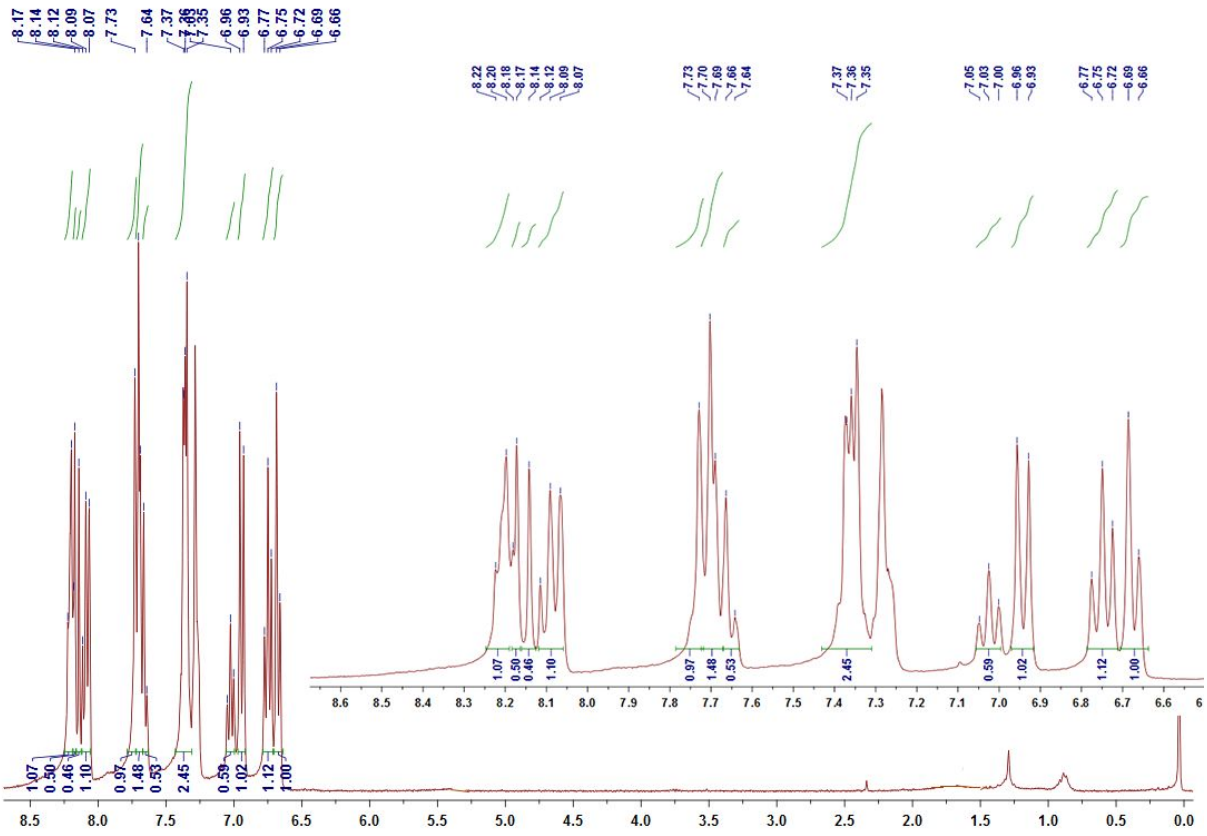

Figure S1. ^{1}H NMR spectra of ICz-DPS

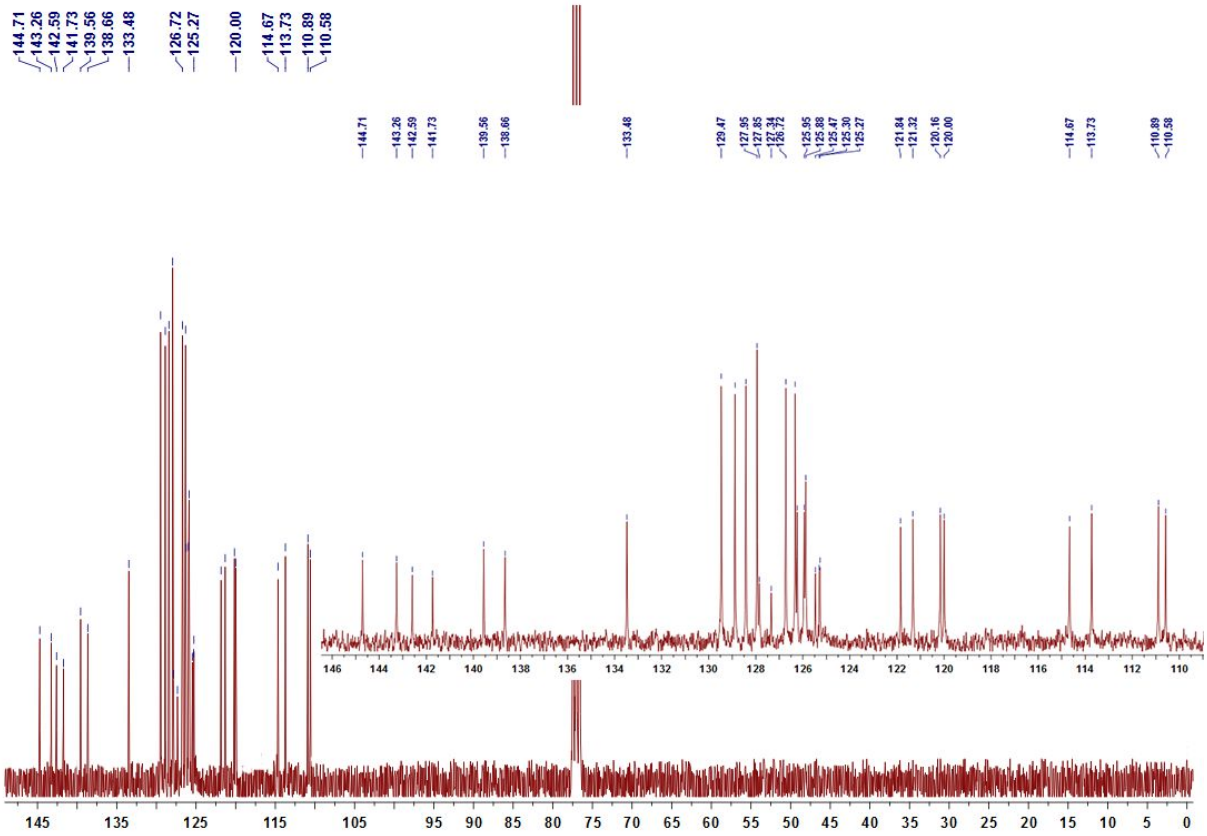

Figure S2. ^{13}C NMR spectra of ICz-DPS

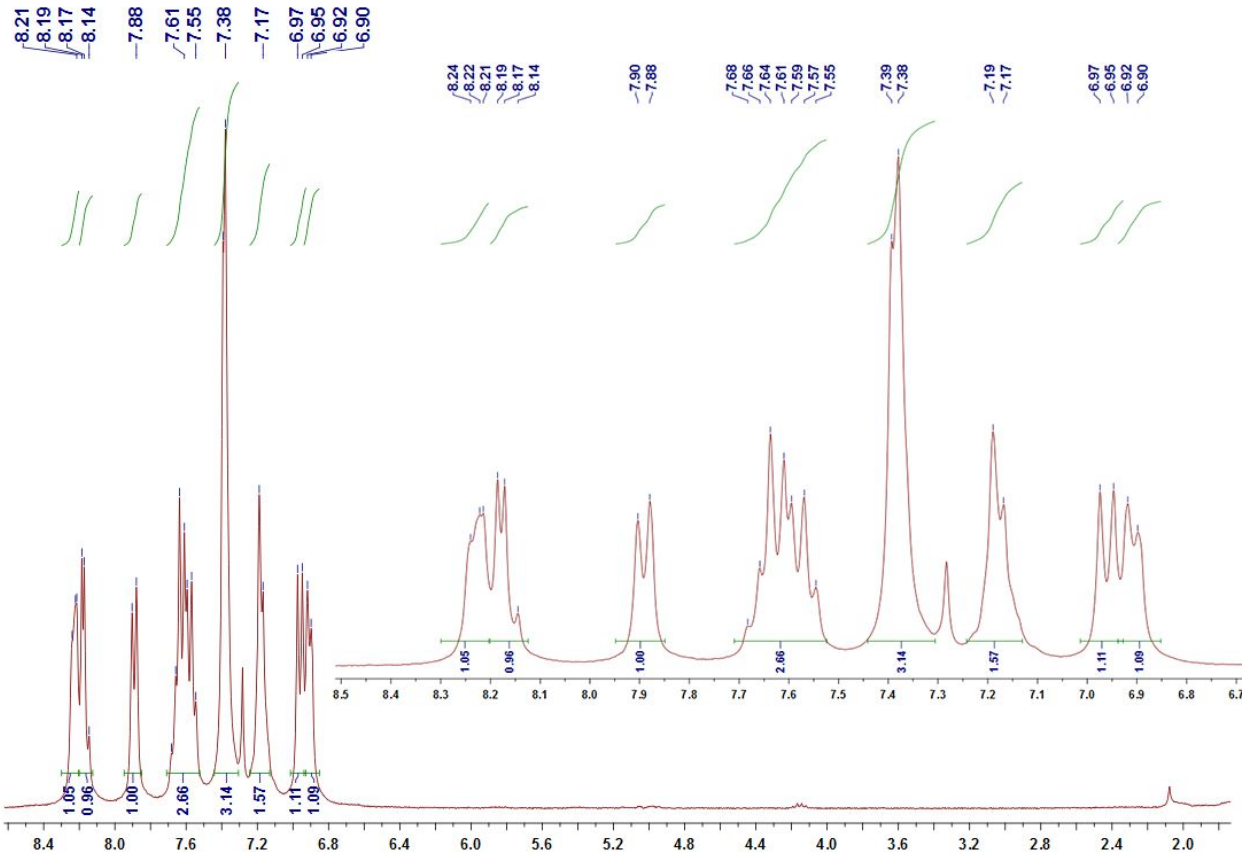

Figure S3. ^{1}H NMR spectra of ICz-BP

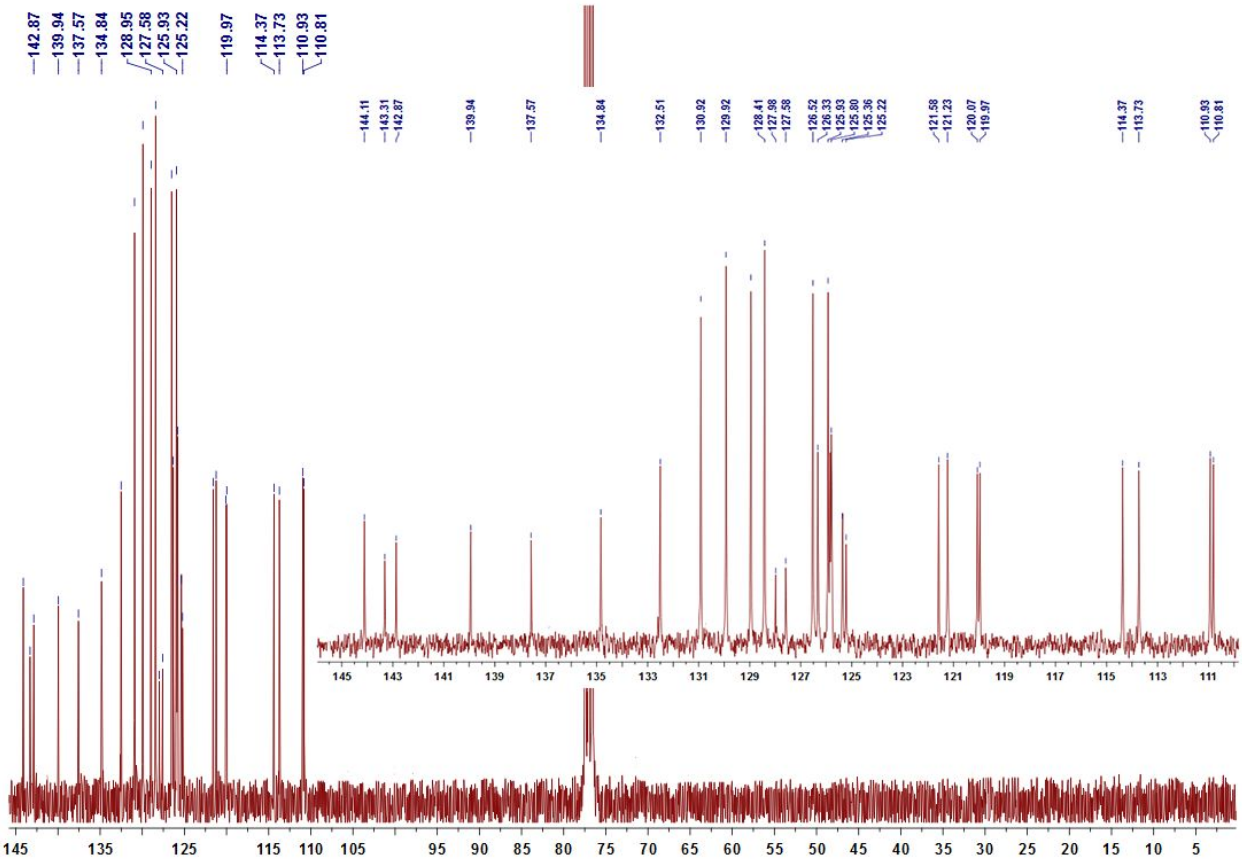

Figure S4. ^{13}C NMR spectra of ICz-BP

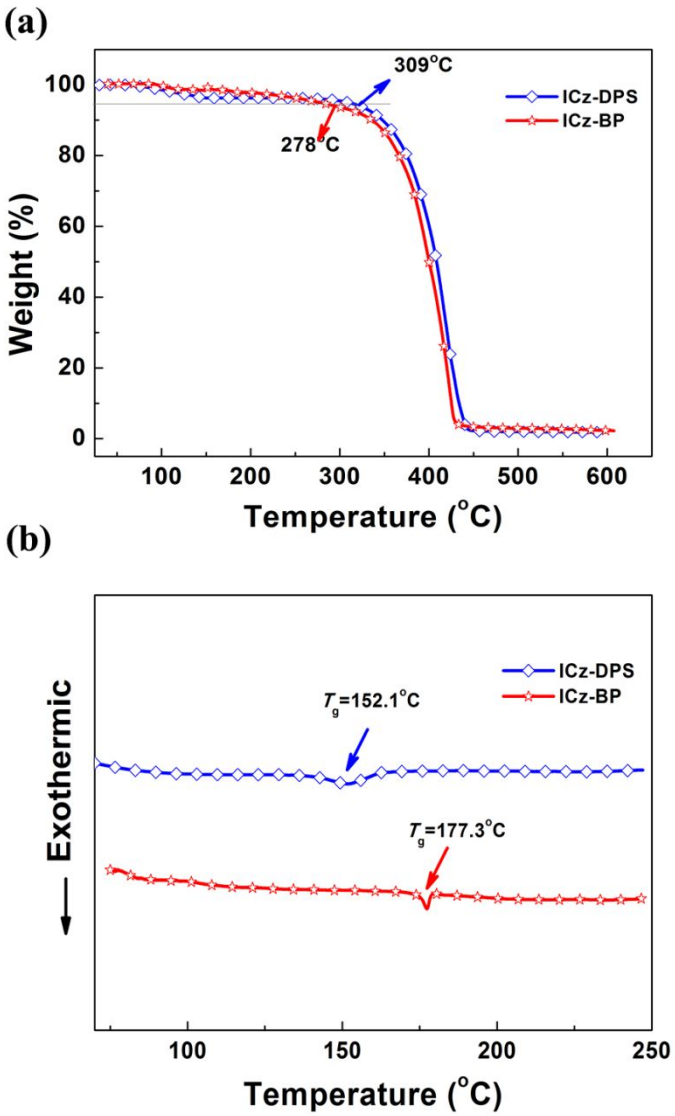

Figure S5. (a) TGA and (b) DSC curves of ICz-DPS and ICz-BP.

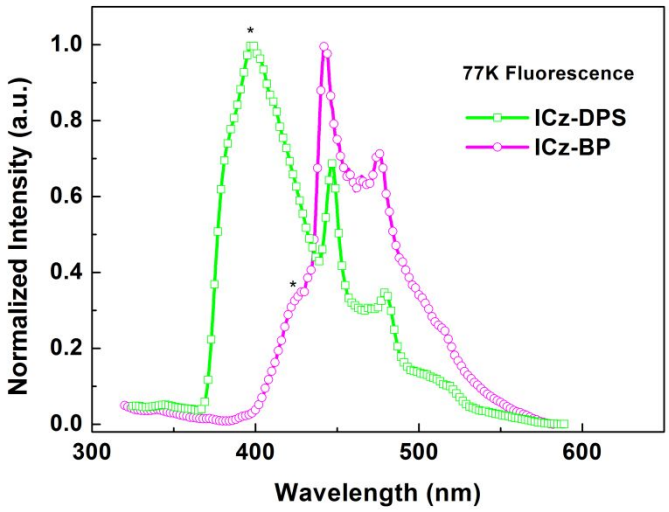

Figure S6. The fluorescence spectra in toluene solution at 77 K.

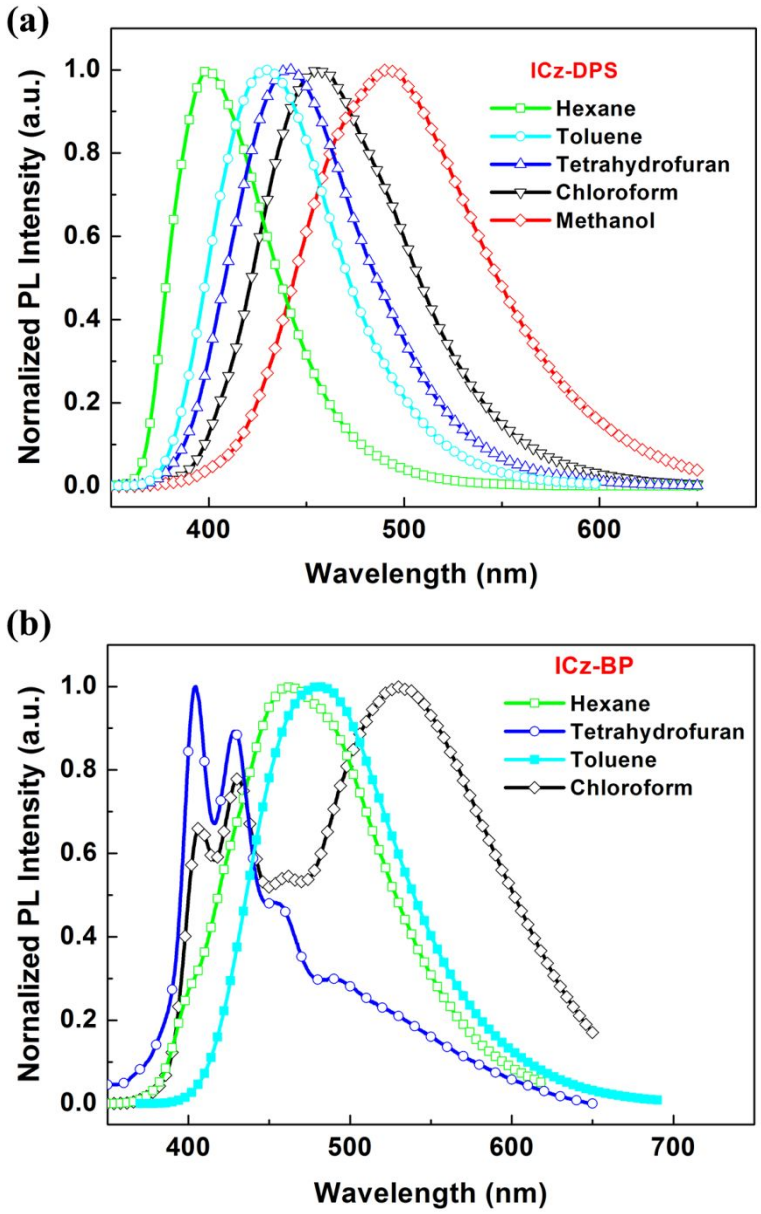

Figure S7. The normalized PL spectra of ICz-DPS (a) and ICz-BP (b) in different solvent.

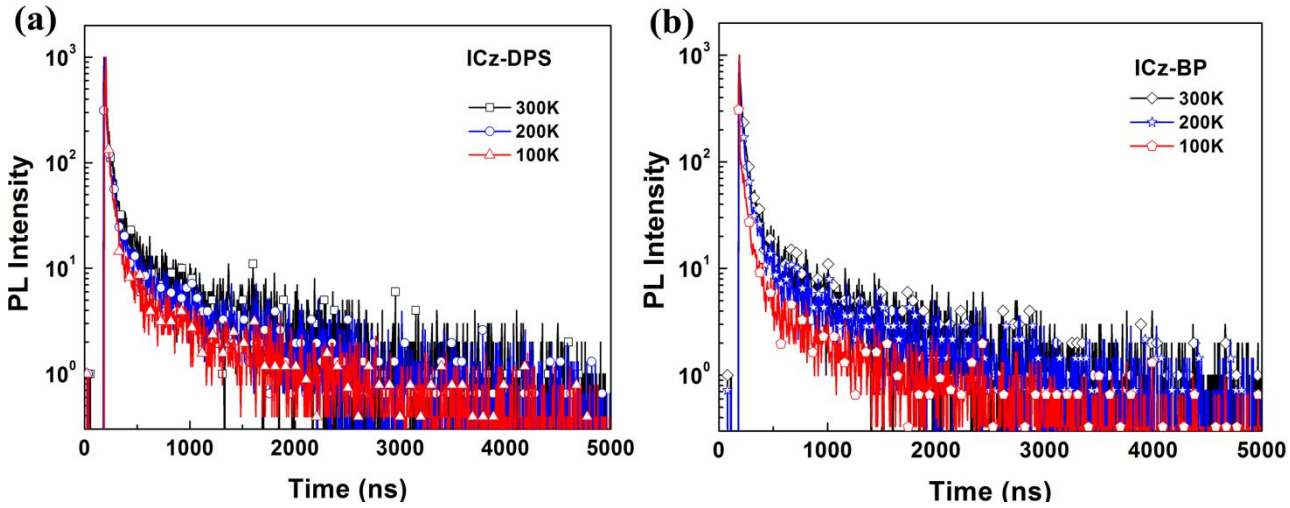

Figure S8. The temperature-dependent PL transient decay spectra of the (a) ICz-DPS and (b) ICz-BP in the neat films from 100 to 300 K. Excitation wavelength: 370 nm nm; detection wavelength: 440 nm for ICZ-DPS and 480 nm for ICZ-BP.

Table S1. Transient PL decay data of neat films and doped films in DPEPO (10 *w*t%) of ICz-DPS and ICz-BP at 300 K under vacuum.

compound	state	Φ_{PL}	τ_p [ns]	τ_d [ns]	B_1	B_2	R_p [%]	R_d [%]
ICz-DPS	neat film	53	21.64	545.98	831.7	21.99	59.99	40.01
	10 *w*t% in DPEPO	71	22.67	616.1	604.1	23.22	48.9	51.1
ICz-BP	neat film	62	20.32	405.60	873.03	26.68	62.12	37.88
	10 *w*t% in DPEPO	80	21.14	447.54	322.5	21.74	41.2	58.8

The transient PL decay data were fitted by double-exponential function. R_p and R_d are individual component ratio for prompt and delayed fluorescence. $Rp = \tau_p B_1/(\tau_p B_1 + \tau_d B_2)$, $R_d = 1 - R_p$, where B_i is the pre-exponential for lifetime τ_i.

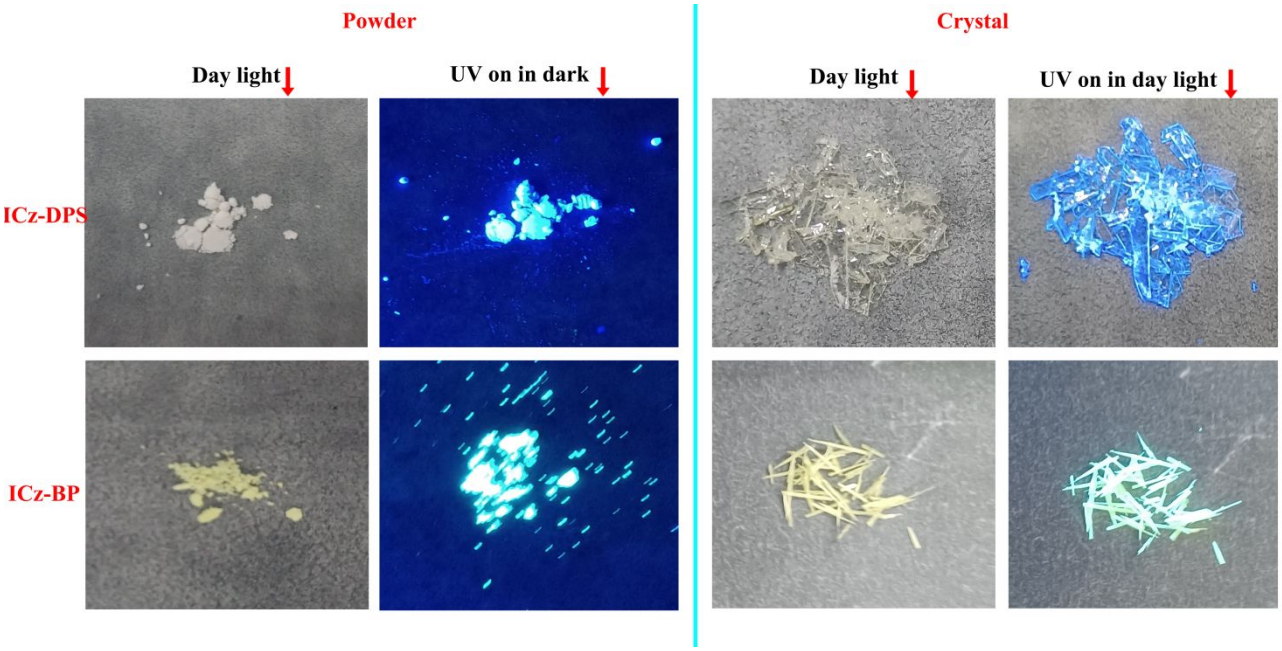

Figure S9. Powders and crystals picture of ICz-DPS and ICz-BP under ultraviolet irradiation (365 nm) and after removal of UV in day light.

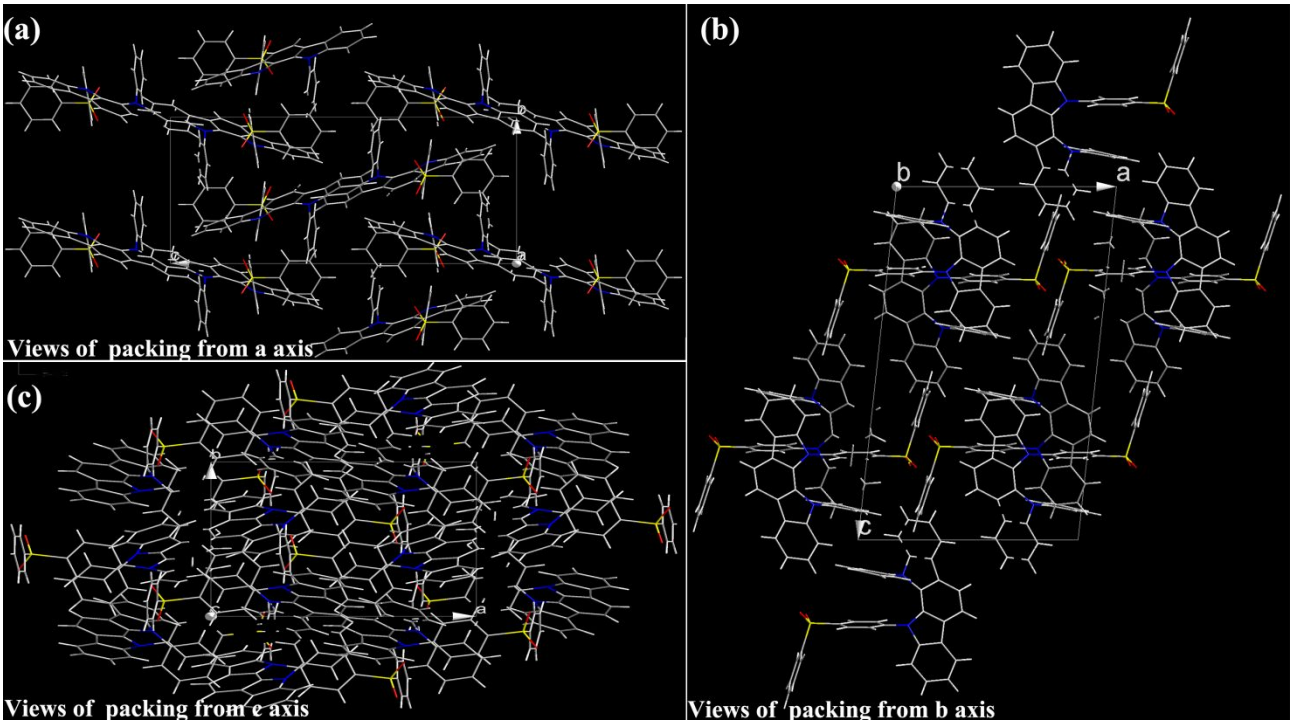

Figure S10. Views of molecular packing of ICz-DPS from (a) *a* axis, (b) *b* axis and (c) *c* axis, respectively.

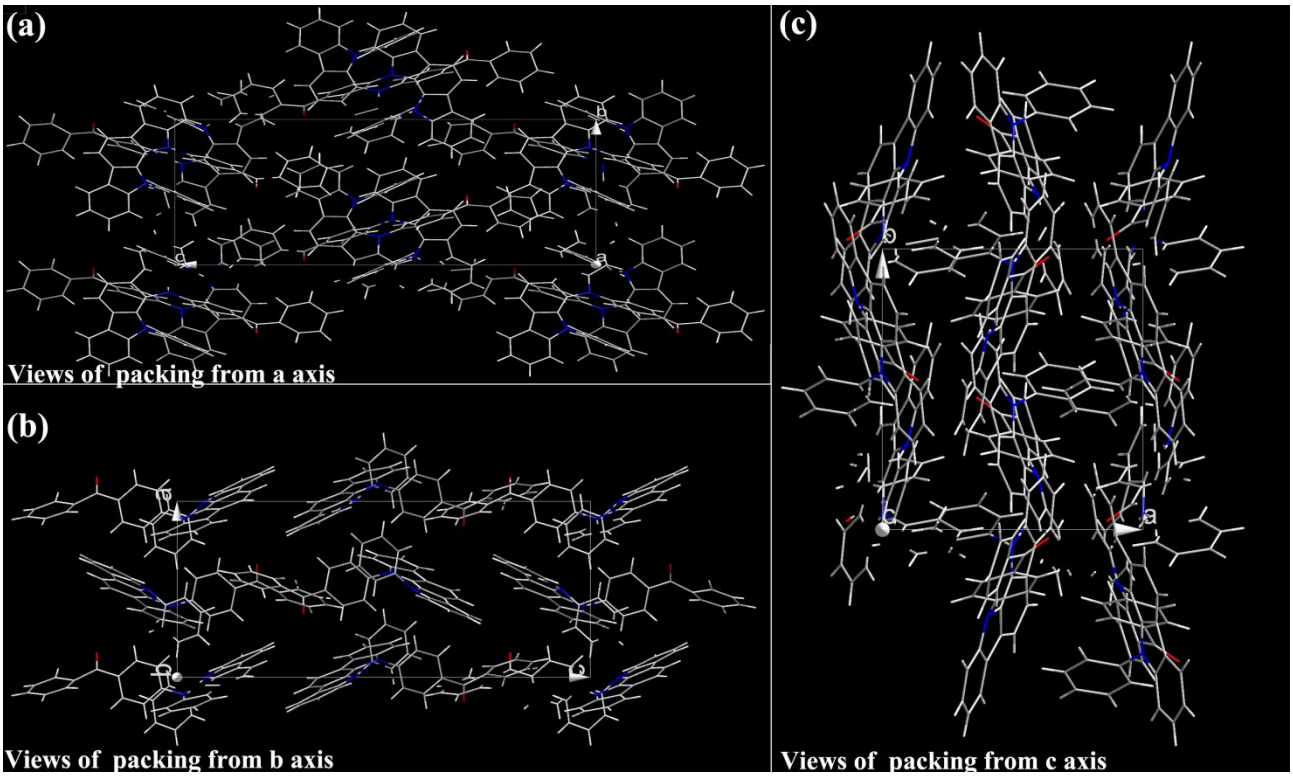

Figure S11. Views of molecular packing of ICz-BP from (a) *a* axis, (b) *b* axis and (c) *c* axis, respectively.

Table S2. Crystal data and structure refinement for ICz-DPS and ICz-BP.

Identification code	ICz-DPS	ICz-BP
Empirical formula	$C_{36}H_{24}N_2O_2S$	$C_{37}H_{24}N_2O$
CCDC number	2094560	2094555
Formula weight	548.66	512.61
Temperature	293 K	293K
Wavelength	1.54184 Å	1.54184 Å
Crystal system	Monoclinic	Orthorhombic
Space group	$P2_1/c$	$P2_12_12_1$
Unit cell dimensions	a = 13.2158(2) Å α= 90° b = 10.7356(2) Å β= 96.074(2)° c = 21.7963(3) Å γ = 90°	a = 10.6909(3) Å α=90° b = 11.5146(5) Å β=90° c = 23.3458(6) Å γ =90°
Volume	3075.09(9) Å3	2873.91(17) $Å^3$
Z	4	4
Density (calculated)	1.279 Mg/m3	1.039 Mg/m^3
Absorption coefficient	1.600 mm-1	0.561 mm^{-1}
F(000)	1228	936
Crystal size	0.16×0.12×0.05 mm^3	0.15×0.03×0.03 mm^3
Theta range for data collection	3.744 to 68.236°.	3.787 to 68.096°.
Index ranges	-15<=h<=14, -12<=k<=12, -21<=l<=26	-12<=h<=12, -13<=k<=13, -28<=l<=21
Reflections collected	31162	29000
Independent reflections	5448 [R(int) = 0.0786]	5117 [R(int) = 0.0521]
Completeness to theta = 67.684°	97.40%	99.90%
Absorption correction	Semi-empirical from equivalents	Semi-empirical from equivalents
Max. and min. transmission	1.00000 and 0.09377	1.00000 and 0.16438
Refinement method	Full-matrix least-squares on F2	Full-matrix least-squares on F2
Data / restraints / parameters	5448 / 0 / 371	5117 / 0 / 361
Goodness-of-fit on F^2	3.307	1.113
Final R indices [I>2sigma(I)]	R1 = 0.2573, wR2 = 0.6154	R1 = 0.0942, wR2 = 0.2649
R indices (all data)	R1 = 0.2628, wR2 = 0.6263	R1 = 0.1096, wR2 = 0.2854
Extinction coefficient	0.008(3)	n/a
Largest diff. peak and hole	6.442 and -0.662 e.$Å^{-3}$	0.787 and -0.283 e.$Å^{-3}$

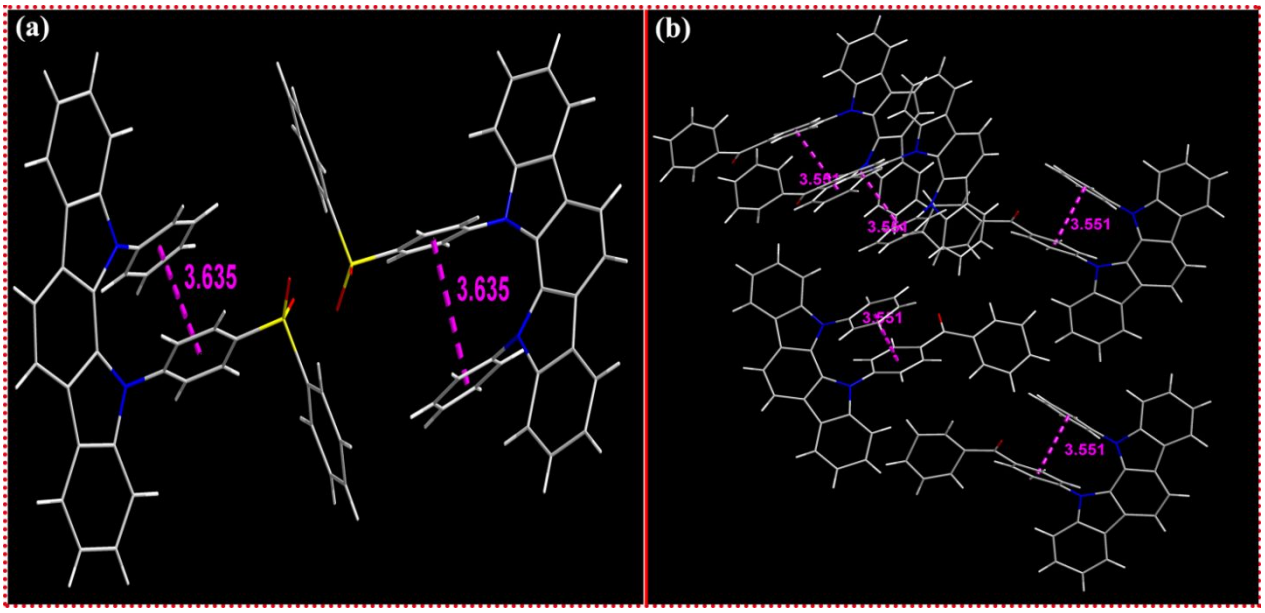

Figure S12. The intramolecular π–π stacking of (a) ICz-DPS and (b) ICz-BP crystals.

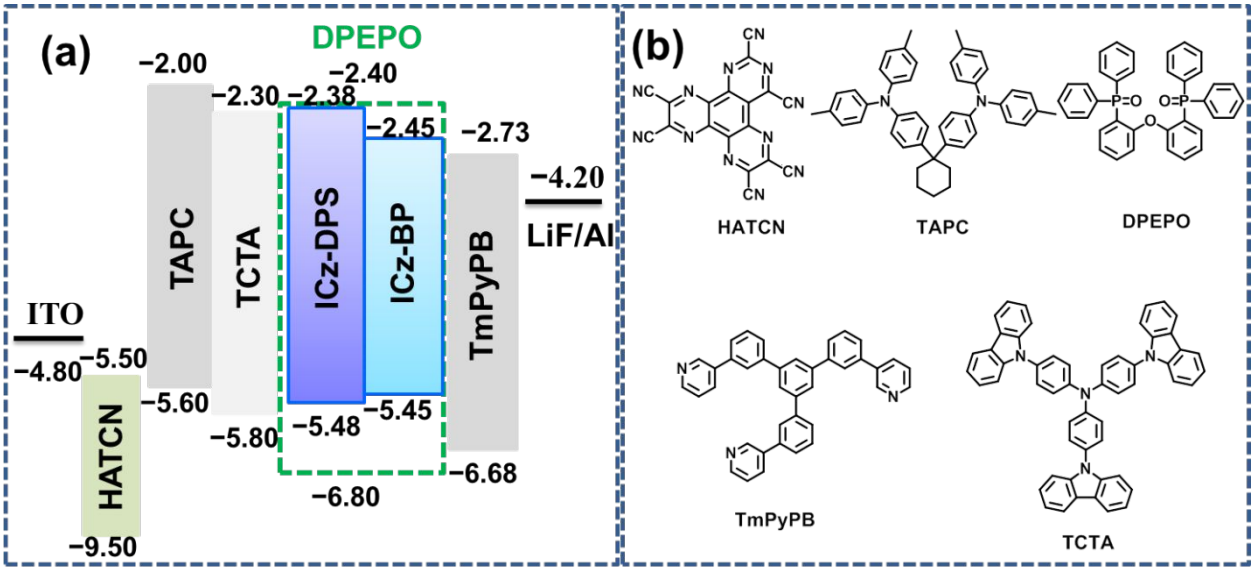

Figure S13. (a) The energy level diagrams of the devices and (b) the molecules used in the devices.

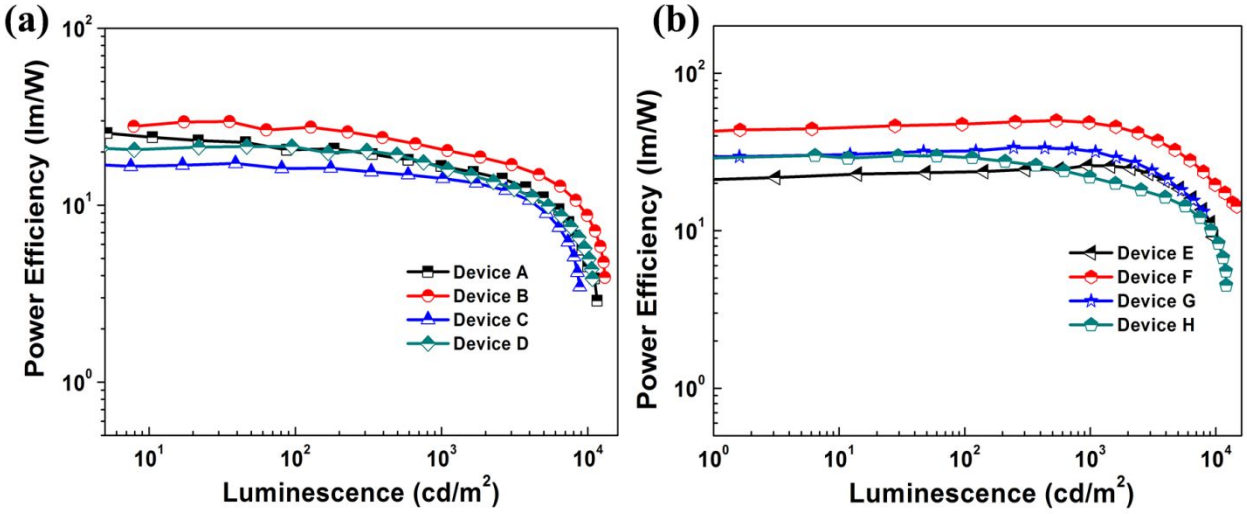

Figure S14. Power efficiency−luminance (η_p−L) characteristics of (a) ICz-DPS devices and (b) ICz-BP devices.

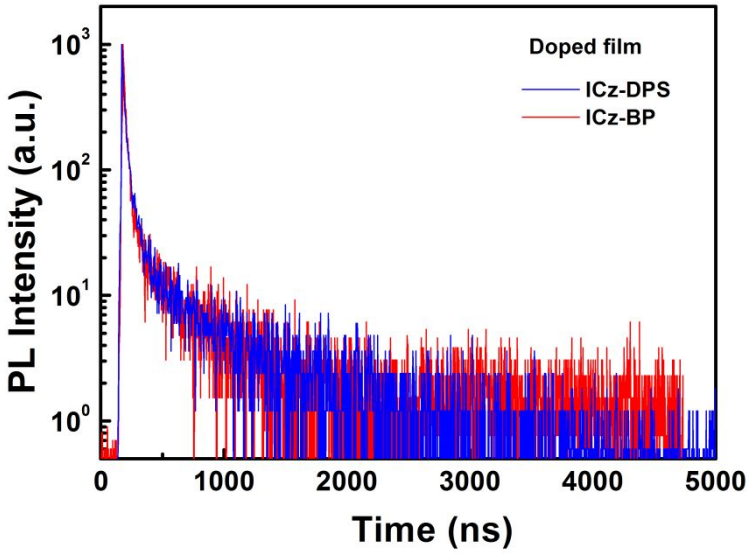

Figure S15. PL transient decay curves of the doped films with dopant concentration of 10*w*t%.

Table S3. The EL performances of doped and nondoped OLEDs in this work and the reported TADF emitters.

EML(Emitter: Host)	Peak [nm]	V_{on}[a)]	η_{ext} (max) [%]	η_{ext} [b)] [%]	η_c [max]	Roll-off[c)] [%]	CIE	Ref.
ICz-DPS:DPEPO	435	3.0	12.8	12.1	30.1	5.4	0.15, 0.08	this
ICz-BP:DPEPO	475	3.2	19.8	19.3	51.4	2.5	0.17, 0.28	work
DMAC-o-TRZ:mCP	496	−	15.5	−	40.0	−	0.20, 0.42	6
TrBACa: C545T	508	3.0	7.13	−	23.83	−	0.27, 0.61	7
CzAc-26DPPM:DPEPO	490	−	23.7	9.28	−	−	0.21, 0.38	8
DBT-BZ-DMAC:CBP	508	3.3	17.9	10.9	51.7	39.8	0.23, 0.51	9
PIAnCN: CzSi		−	6.77	4.77	5.95	29.5	0.15, 0.07	10
MXAc-BF:PPF	478	3.0	16.2	12.0	−	25.9	0.17, 0.29	11
oBFCzTrz :DPEPO	480	−	20.4	−	−	−	0.18, 0.31	12
5CzBN:mCBP	490	−	16.7	9.8 @500cd/m^2	−	41.3	0.22, 0. 40	13
5TCzBN:mCBP	490	−	21.2	10.7 @500cd/m^2	−	49.5	0.21, 0.41	13
DDCzTrz:DPEPO	467	−	18.9	5.5 @500cd/m^2	−	70.8	0.16, 0.22	14
DCzTrz:DPEPO	459	−	17.8	14.9 @500cd/m^2	−	16.3	0.15, 0.16	14
2QPM-mDC :mCBP	498	3.5	17.5	−	46.6	−	0.19, 0.46	15
2QPM-mDTC: mCBP	514	3.5	24	15.5 @500cd/m^2	79.5	35	0.25, 0.56	15
III:DPEPO	461	−	22.6	19.9	−	11.9	0.15, 0.18	16
BCzTrz:DPEPO	490	−	23.6	5.2	53.3		0.23, 0.42	17
TCzTrz:DPEPO	510	−	31.8	11.3	86.4		0.20, 0.44	17
SpiroAC-TRZ: mCPCN	490	−	36.7	30.5	94	16.9	−	18
				Nondoped				
DBT-BZ-DMAC	508	2.7	14.2	14.2	43.3	0.46	0.26, 0.55	9
PIAnCN	−	−	9.44	9.44	13.16	0	0.14, 0.19	10
DMAC–BP	−	2.6	18.9	18.0	−	4.8	−	19
PyPPA	464	2.8	8.47		9.16		0.14, 0.13	20
ICz-DPS	440	2.7	9.6	9.0	25.2	6.3	0.15, 0.09	this
ICz-BP	480	3.1	10.7	9.9	31.6	7.5	0.18, 0.30	work

a)Turn-on voltage at 1 cd m^{-2}. b) External quantum efficiency at the luminance of 1000 cd m^{-2}. c) RO = EQE roll-off from peak value to that at 1000 cd m^{-2}.

6. References

(1) Lee, S. Y.; Yasuda, T.; Yang, Y. S.; Zhang, Q.; Adachi, C. Luminous Butterflies: Efficient Exciton Harvesting by Benzophenone Derivatives for Full−Color Delayed Fluorescence OLEDs. *Angew. Chem. Int. Ed.* **2014**, 53, 6402−6406.

(2) Zhang, Q.; Kuwabara, H.; Potscavage, W. J.; Huang, Jr. S.; Hatae, Y.; Shibata, T.; Adachi, C. Anthraquinone-Based Intramolecular Charge-Transfer Compounds: Computational Molecular Design, Thermally Activated Delayed Fluorescence, and Highly Efficient Red Electroluminescence. *J. Am. Chem. Soc.* **2014**, 136, 18070−18081.

(3) Hirata, S.; Sakai, Y.; Masui, K.; Tanaka, H.; Lee, S. Y.; Nomura, H.; Nakamura, N.; Yasumatsu, M.; Nakanotani, H.; Zhang, Q.; Shizu, K.; Miyazaki, H.; Adachi, C. Highly Efficient Blue Electroluminescence Based on Thermally Activated Delayed Fluorescence. *Nature Mater.* **2015**, 14, 330−336.

(4) Nakagawa, T.; Ku, S.-Y.; Wong, K.-T.; Adachi, C.; Electroluminescence Based on Thermally Activated Delayed Fluorescence Generated by a Spirobifluorene Donor–Acceptor Structure. *Chem. Commun.* **2012**, 48, 9580−9582.

(5) Park, I. S.; Lee, S. Y.; Adachi, C.; Yasuda, T. Full-Color Delayed Fluorescence Materials Based on Wedge-Shaped Phthalonitriles and Dicyanopyrazines: Systematic Design, Tunable Photophysical Properties, and OLED Performance. *Adv. Funct. Mater.* **2016**, 26, 1813−1821.

(6) Shi, Y.-Z.; Wang, K.; Li, X.; Dai, G.-L.; Liu, W.; Ke, K.; Zhang, M.; Tao, S.-L.; Zheng, C.-J.; Ou, X.-M.; Zhang, X.-H. Intermolecular Charge-Transfer Transition Emitter Showing Thermally Activated Delayed Fluorescence for Efficient Non-Doped OLEDs. *Angew. Chem. Int. Ed.* **2018**, 57, 9480 –9484.

(7) Yu, Y.; Ma, L.; Yang, X.; Zhou, H.; Qin, H.; Song, J.; Zhou, G.; Wang, D.; Wu, Z. High Effciency Fluorescent Electroluminescence with Extremely Low Effciency Roll-Off Generated by a Donor-Bianthracene-Acceptor Structure: Utilizing Perpendicular Twisted Intramolecular Charge Transfer Excited State, Adv. Optical Mater. 2018, 6, 1800060.

(8) Nakao, K.; Sasabe, H.; Komatsu, R.; Hayasaka, Y.; Ohsawa, T; Kido, J. Signifcant Enhancement of Blue OLED Performances through Molecular Engineering of Pyrimidine-Based Emitter. *Adv. Optical* Mater. **2017**, 5, 1600843.

(9) Guo, J.; Li, X.-L.; Nie, H.; Luo, W.; Gan, S.; Hu, S.; Hu, R.; Qin, A.; Zhao, Z.; Su, S.-J.; Tang, B. Z. Achieving High-Performance Nondoped OLEDs with Extremely Small Efficiency Roll-Off by Combining Aggregation-Induced Emission and Thermally Activated Delayed Fluorescence. *Adv. Funct. Mater.* **2017**, 27, 1606458.

(10) Tang, X.; Bai, Q.; Shan, T.; Li, J.; Gao, Y.; Liu, F.; Liu, H.; Peng, Q.; Yang, B.; Li, F.; Lu, P. Efficient Nondoped Blue Fluorescent Organic Light-Emitting Diodes (OLEDs) with a High External Quantum Efficiency of 9.4% @ 1000 cd m^{-2} Based on Phenanthroimidazole-Anthracene Derivative. *Adv. Funct. Mater.* **2018**, 28, 1705813.

(11) Lee, J.; Aizawa, N.; Yasuda, T.; Isobenzofuranone- and Chromone-Based Blue Delayed Fluorescence Emitters with Low Efficiency Roll-Off in Organic Light-Emitting Diodes. *Chem. Mater.* **2017**, 29, 8012−8020.

(12) Lee, D. R.; Choi, J. M.; Lee, C. W.; Lee, J. Y.; Ideal Molecular Design of Blue Thermally Activated Delayed Fluorescent Emitter for High Efficiency, Small Singlet-Triplet Energy Splitting, Low Efficiency Roll-Off, and Long Lifetime. *ACS Appl. Mater. Interfaces* **2016**, 8, 23190−23196.

(13) Zhang, D.; Cai, M.; Zhang, Y.; Zhang, D.; Duan, L.; Sterically Shielded Blue Thermally Activated Delayed Fluorescence Emitters with Improved Efficiency and Stability. *Mater. Horiz.* **2016**, 3, 145−151.

(14) Kim, M.; Jeon, S. K.; Hwang, S.-H.; Lee, J. Y.; Stable Blue Thermally Activated Delayed Fluorescent Organic Light-Emitting Diodes with Three Times Longer Lifetime than Phosphorescent Organic Light-Emitting Diodes. *Adv. Mater.* **2015**, 27, 2515–2520.

(15) Thangaraji, V.; Rajamalli, P.; Jayakumar, J.; Huang, M.-J.; Chen, Y.-W.; Cheng, C.-H.; Quinolinylmethanone-Based Thermally Activated Delayed Fluorescence Emitters and the Application in OLEDs: Effect of Intramolecular H-Bonding. *ACS Appl. Mater. Interfaces* **2019**, 11, 17128−17133.

(16) Stachelek, P.; Ward, J. S.; Dos Santos, P. L.; Danos, A.; Colella, M.; Haase, N.; Raynes, S. J.; Batsanov, A. S.; Bryce, M. R.; Monkman, A. P. Molecular Design Strategies for Color Tuning of Blue TADF Emitters. *ACS Appl. Mater. Interfaces* **2019**, 11, 27125−27133.

(17) Byeon, S. Y.; Kim, J.; Lee, D. R.; Han, S. H.; Forrest, S. R.; Lee, J. Y. Nearly 100% Horizontal Dipole Orientation and Upconversion Effciency in Blue Thermally Activated Delayed Fluorescent Emitters. *Adv. Optical Mater.* **2018**, 6, 1701340.

(18) Lin, T.-A.; Chatterjee, T.; Tsai, W.-L.; Lee, W.-K.; Wu, M.-J.; Jiao, M.; Pan, K.-C.; Yi, C.-L.; Chung, C.-L.; Wong, K.-T.; Wu, C.-C. Sky-Blue Organic Light Emitting Diode with 37% External Quantum Efficiency Using Thermally Activated Delayed Fluorescence from Spiroacridine-Triazine Hybrid. *Adv. Mater.* **2016**, 28, 6976−6983.

(19) Zhang, Q.; Tsang, D.; Kuwabara, H.; Hatae, Y.; Li, B.; Takahashi, T.; Lee, S. Y.; Yasuda, T.; Adachi, C. Nearly 100% Internal Quantum Efficiency in Undoped Electroluminescent Devices Employing Pure Organic Emitters. *Adv. Mater.* **2015**, 27, 2096−2100.

(20) Liu, Y.; Liu, H.; Bai, Q.; Du, C.; Shang, A.; Jiang, D.; Tang, X.; Lu, P. Pyrene[4,5-d]imidazole-Based Derivatives with Hybridized Local and Charge-Transfer State for Highly Efficient Blue and White Organic Light-Emitting Diodes with Low Efficiency Roll-Off. *ACS Appl. Mater. Interfaces* **2020**, 12, 16715−16725.